Radionuclide Tumor Targeting Using ADAPT Scaffold Proteins: Aspects of Label Positioning and Residualizing Properties of the Label

Sarah Lindbo*[1], Javad Garousi*[2], Bogdan Mitran[3], Mohamed Altai[2], Jos Buijs[2], Anna Orlova[3], Sophia Hober[1], and Vladimir Tolmachev[2]

[1]School of Biotechnology, Division of Protein Technology, KTH Royal Institute of Technology, Stockholm, Sweden; [2]Institute for Immunology, Genetics and Pathology, Uppsala University, Uppsala, Sweden; and [3]Division of Molecular Imaging, Department of Medicinal Chemistry, Uppsala University, Uppsala, Sweden

Visualization of cancer-associated alterations of molecular phenotype using radionuclide imaging is a noninvasive approach to stratifying patients for targeted therapies. The engineered albumin-binding domain–derived affinity protein (ADAPT) is a promising tracer for radionuclide molecular imaging because of its small size (6.5 kDa), which satisfies the precondition for efficient tumor penetration and rapid clearance. Previous studies demonstrated that the human epidermal growth factor receptor type 2 (HER2)–targeting ADAPT6 labeled with radiometals at the N terminus is able to image HER2 expression in xenografts a few hours after injection. The aim of this study was to evaluate whether the use of a nonresidualizing label or placement of the labels at the C terminus would further improve the targeting properties of ADAPT6. **Methods:** Two constructs, Cys[2]-ADAPT6 and Cys[59]-ADAPT6, having the $(HE)_3DANS$ sequence at the N terminus were produced and site-specifically labeled using ^{111}In-DOTA or ^{125}I-iodo-((4-hydroxyphenyl) ethyl) maleimide (HPEM). The conjugates were compared in vitro and in vivo. HER2-targeting properties and biodistribution were evaluated in BALB/C nu/nu mice bearing ovarian carcinoma cell (SKOV-3) xenografts. **Results:** Specific HER2 binding and high affinity were preserved after labeling. Both Cys[2]-ADAPT6 and Cys[59]-ADAPT6 were internalized slowly by HER2-expressing cancer cells. Depending on the label position, uptake at 4 h after injection varied from 10% to 22% of the injected dose per gram of tumor tissue. Regardless of terminus position, the ^{125}I-HPEM label provided more than 140-fold lower renal uptake than the ^{111}In-DOTA label at 4 after injection. The tumor-to-organ ratios were, in contrast, higher for both of the ^{111}In-DOTA–labeled ADAPT variants in other organs. Tumor-to-blood ratios for ^{111}In-labeled Cys[2]-ADAPT6 and Cys[59]-ADAPT6 did not differ significantly (250–280), but ^{111}In-DOTA-Cys[59]-ADAPT6 provided significantly higher tumor-to-lung, tumor-to-liver, tumor-to-spleen, and tumor-to-muscle ratios. Radioiodinated variants had similar tumor-to-organ ratios, but ^{125}I-HPEM-Cys[59]-ADAPT6 had significantly higher tumor uptake and a higher tumor-to-kidney ratio. **Conclusion:** Residualizing properties of the label strongly influence the targeting properties of ADAPT6. The position of the radiolabel influences targeting as well, although to a lesser extent. Placement of a label at the C terminus yields the best biodistribution features for both radiometal and radiohalogen labels. Low renal retention of the radioiodine label creates a precondition for radionuclide therapy using ^{131}I-labeled HPEM-Cys[59]-ADAPT6.

Key Words: molecular biology; ADAPT; HER2; biodistribution; molecular imaging; terminal sequence

Targeting molecular abnormalities on cancer cells is an attractive treatment strategy because it minimizes damage to normal tissues. Antibodies against cancer-associated antigens or receptors that are overexpressed in malignant tumors improve survival of patients in the clinic (1). However, tumor cells of the same origin might have different molecular phenotypes that require different targeting agents. Thus, to be successful, targeted therapy needs to be customized for every patient, thus requiring the development of a methodology for the exact molecular characterization of the tumor. Radionuclide molecular imaging is a promising approach for visualization of therapeutic targets. This method allows whole-body detection and is noninvasive, as opposed to biopsy-based diagnosis (2,3). One strategy is to use the therapeutic antibodies labeled with the positron-emitting radionuclide [89]Zr (4). Although these antibodies bind very specifically to their targets, the unbound fraction clears slowly from the blood, making it necessary to wait several days before images of sufficient quality can be achieved. Another potential limitation of full-length antibody-based imaging probes is their unspecific accumulation in tumors (4) due to the enhanced permeability and retention effect, as is typical for globular proteins with a molecular weight of more than 45 kDa (5). These issues are related to the large size of the antibodies.

Small engineered scaffold proteins recently emerged as a promising format for targeted probes for radionuclide molecular imaging. Affibody molecules have already demonstrated excellent sensitivity and specificity in clinical studies (6,7). Other scaffold proteins, such as designed ankyrin repeat proteins and cystine-knot miniproteins, have undergone preclinical evaluation (8,9). Still, our knowledge about factors influencing the sensitivity and specificity of imaging using engineered scaffold proteins is insufficient. Therefore, extensive studies are required to exploit the full potential of these imaging agents.

We earlier demonstrated the feasibility of high-contrast molecular imaging using albumin-binding domain–derived affinity proteins (ADAPTs) (10). ADAPTs are small (6.5 kDa) engineered scaffold proteins derived from the albumin-binding domain of streptococcal protein G (11). These 3-helix scaffold proteins are approximately 20 times smaller than an IgG antibody, thus providing more efficient extravasation, faster tumor penetration, and faster clearance of unbound molecules from blood. Validation of ADAPTs as an imaging probe was performed using a binder specific to the human epidermal growth factor receptor type 2 (HER2) receptor. Treatment with anti-HER2 monoclonal antibodies significantly improves survival of patients with HER2-overexpressing breast cancer (12). However, the success of the treatment depends on the intensity of HER2 expression, and approximately only 20% of the tumors have sufficient levels.

We demonstrated that radiolabeled anti-HER2 ADAPT6 provides high-contrast images a few hours after injection (10,13,14). Studies concerning the influence of the N-terminal sequence on the biodistribution of ADAPT6 have shown that introduction of an (HE)$_3$DANS sequence at the N terminus provides the highest-contrast imaging of HER2 expression in human xenografts in mice (13). However, all previous ADAPT6 variants were labeled using radiometals (^{111}In, ^{99m}Tc, or ^{68}Ga), and the labels were site-specifically placed at the N terminus (10,13,14). The position of a label is essential because it influences local charge and lipophilicity, which might affect both affinity to the intended target and the propensity of off-target interaction with normal tissues, thereby modifying the imaging contrast. Earlier, the impact of label position was demonstrated for short peptides (15) and Affibody molecules (16–18).

Another important factor is the residualizing properties of a label, that is, the degree of intracellular trapping of radiometabolites after internalization of a tracer and their degradation in the lysosomes. Internalization of all tested ADAPT6 variants by cancer cells is slow. Therefore, residualization of a label is not critical for retention of radioactivity in tumors. On the other hand, strong residualization of radiometals causes prolonged retention of radiometabolites in the kidneys. This is essential, as ADAPT6 is efficiently reabsorbed in the proximal tubules and the reabsorption cannot be reduced by coinjection of L-lysine or Gelofusine (B. Braun Medical AG) (14). High renal uptake has been observed for all tested ADAPT6 constructs and is a general feature of small scaffold proteins labeled with radiometals (8,17,19). The high retention of radiometals in the kidneys prevents the use of radiometal-labeled ADAPT6 for radionuclide therapy. Nonresidualizing radiohalogens diffuse from the cell after lysosomal degradation because of their lipophilic nature

(19). The slow internalization of ADAPT in tumor cells but rapid internalization in the kidneys makes radiohalogen labels an attractive alternative by providing a potentially better tumor-to-kidney ratio.

Therefore, our goal was to investigate whether the use of a nonresidualizing label or C-terminal positioning of the labels would improve the biodistribution. In this study, we labeled (HE)$_3$DANS-ADAPT6 at the N and C terminus with ^{111}In-DOTA or ^{125}I-iodo-((4-hydroxyphenyl)ethyl) maleimide (HPEM) (Fig. 1) for a direct comparison of the influence of the different properties of the radionuclides and the position of the label.

MATERIALS AND METHODS

Data on cellular uptake and biodistribution were analyzed by unpaired 2-tailed t testing using Prism (version 4.00 for Microsoft Windows; GraphPad Software) to determine significant differences ($P < 0.05$) when 2 groups were compared. Biodistribution data concerning dual-label studies were analyzed using paired t testing.

Radiolabeled ADAPT6 variants

ADAPT6 variants containing the (HE)$_3$DANS sequence at the N terminus and a cysteine either at the N terminus (denoted Cys^2-ADAPT6) or the C terminus (denoted Cys^{59}-ADAPT6) (Fig. 1) were produced, purified, and characterized as described earlier (10). The constructs intended for ^{111}In labeling were conjugated with maleimide-DOTA (Macrocyclics) to the thiol group of the terminal cysteines and designated DOTA-Cys^2-ADAPT6 and DOTA-Cys^{59}-ADAPT6.

DOTA-Cys^2-ADAPT6 and DOTA-Cys^{59}-ADAPT6 were labeled with ^{111}In, and their stability was evaluated according to methods described earlier (10).

HPEM was synthesized and characterized using a method described earlier (20). HPEM-Cys^2-ADAPT6 and HPEM-Cys^{59}-ADAPT6 were labeled with [125]I (Fig. 1) according to a method described earlier for Affibody molecules (21).

In Vitro Evaluation

The specificity of binding of the radiolabeled ADAPT6 derivatives to HER2-expressing cancer cells was tested using SKOV-3 and breast carcinoma BT474 cell lines using a saturation method described earlier (22).

The affinity of radiolabeled conjugates binding to HER2-expressing SKOV-3 cells was determined using LigandTracer (Ridgeview Instruments AB) as described previously (23).

The pattern of ^{111}In-DOTA-Cys^2-ADAPT6 and ^{111}In-DOTA-Cys^{59}-ADAPT6 internalization by SKOV-3 and BT474 cells during continuous incubation was studied using the acid wash method (22).

In Vivo Studies

Animal studies were planned in agreement with Swedish national legislation concerning protection of laboratory animals and were approved by the Ethics Committee for Animal Research in Uppsala.

The targeting properties of ^{111}In-DOTA-Cys^2-ADAPT6, ^{111}In-DOTA-Cys^{59}-ADAPT6, ^{125}I-HPEM-Cys^2-ADAPT6, and ^{125}I-HPEM-Cys^{59}-ADAPT6 were evaluated in BALB/C *nu/nu* mice bearing SKOV-3 xenografts. Xenografts were established by subcutaneous implantation of 10^7 SKOV-3 cells. To reduce the number of tumor-bearing mice required, a dual-label approach was used. The animals were intravenously (tail vein) injected with a mixture of [125]I- and ^{111}In-labeled ADAPT6
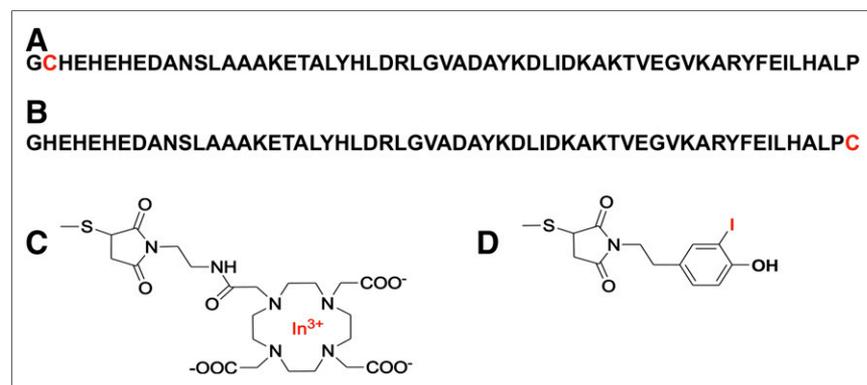

FIGURE 1. Structures of Cys^2-ADAPT6 (A), Cys^{59}-ADAPT6 (B), maleimido-DOTA (C), and HPEM (D) conjugated to cysteine.

(15 kBq of both ^{125}I and ^{111}In per animal in 100 μL of phosphate-buffered saline). The total injected protein dose was adjusted to 3 μg/mouse using the corresponding nonlabeled ADAPT6.

To test whether tumor uptake of ^{111}In-DOTA-Cys[59]-ADAPT6 and ^{125}I-HPEM-Cys[59]-ADAPT6 was HER2-specific, receptors in a control group were saturated by injection of 15 mg of trastuzumab per animal 24 h before injection of radiolabeled ADAPT6. Biodistribution in non-saturated animals was measured at 1 and 4 h after injection. Biodistribution in the control group was measured at 4 h after injection. Euthanasia was performed under xylazine/ketamine anesthesia. The tissue samples were weighed, and their radioactivity was measured using an automated γ-spectrometer. Radioactivity was measured in the energy window from 5 to 90 keV for ^{125}I and from 115 to 600 keV for [111]In. The data were corrected for dead time, spillover, and background.

The contribution of blood-borne radiometabolites to the blood radioactivity concentration was assessed by size-exclusion analysis.

Whole-body SPECT/CT scans of the mice injected with ^{125}I-labeled HPEM-Cys[2]-ADAPT6 and HPEM-Cys[59]-ADAPT6 (3 μg, 1 MBq) and ^{111}In-labeled DOTA-Cys[2]-ADAPT6 and DOTA-Cys[59]-ADAPT6 (3 μg, 3 MBq) were obtained using a nanoScan SC system (Mediso Medical Imaging Systems) at 4 h after injection.

RESULTS

Radiolabeled ADAPT6 Variants

Two constructs, designated Cys[2]-ADAPT6 and Cys[59]-ADAPT6, were produced in *Escherichia coli* and purified using 90°C heat treatment followed by immobilized-metal affinity chromatography. Proteins intended for ^{111}In labeling were conjugated with maleimide-DOTA. The purity of the constructs was above 99%, determined by reverse-phase high-performance liquid chromatography, and the identities were confirmed by mass spectrometry (Supplemental Fig. 1; supplemental materials are available at http://jnm.snmjournals.org). The circular dichroism analysis showed high α-helical content, melting temperatures of above 61°C, and good refolding properties after heating to 90°C for both constructs (Supplemental Fig. 2). According to the surface plasmon resonance measurements, the position of the cysteine did not affect binding to HER2, because both variants had similar equilibrium dissociation constants (K_D), 2.2 and 2.6 nM for Cys[2]-ADAPT6 and Cys[59]-ADAPT6, respectively, comparable to the parental ADAPT6 molecule (K_D, 2.5 nM).

DOTA-Cys[2]-ADAPT6 and DOTA-Cys[59]-ADAPT6 were labeled with ^{111}In with a yield of 99% ± 1%. The radiochemical purity after size-exclusion chromatography was 100% ± 0%. A challenge with a 500-fold excess of ethylenediaminetetraacetic acid during 4 h did not reveal any release of radionuclide from the conjugates.

The site-specific indirect radioiodination of ADAPT6 using HPEM agreed well with earlier published results for radioiodination of Affibody molecules (Supplemental Fig. 3) (21). The overall yield of radioiodination for Cys[2]-ADAPT6 and Cys[59]-ADAPT6 using HPEM was 35%–48%. The radiochemical purity after size-exclusion chromatography was over 99%. The maximum achieved effective specific radioactivity was 1.1 MBq/μg (7.7 GBq/μmol) and 0.33 MBq/μg (2.15 GBq/μmol) for labeling with ^{111}In and ^{125}I, respectively.

In Vitro Evaluation

The binding of all radiolabeled ADAPT6 variants to both HER2-expressing SKOV-3 cells and HER2-expressing BT474 cells was significantly ($P < 0.0005$) reduced after presaturation of the receptors by nonlabeled ADAPT6, demonstrating that the binding was saturable and confirming its HER2-specific character (Supplemental Fig. 4).

According to LigandTracer measurements, the binding of ^{111}In-DOTA-Cys[2]-ADAPT6, ^{111}In-DOTA-Cys[59]-ADAPT6, ^{125}I-HPEM-Cys[2]-ADAPT6, and ^{125}I-HPEM-Cys[59]-ADAPT6 variants to living cells best fit a 1:2 interaction model, suggesting that there were 2 types of interactions with HER2 having similar association constants but different dissociation rates (Supplemental Fig. 5). The average K_D values were in the range of 0.1–0.2 nM for the first interaction and 3–11 nM for the second. The K_D values for the interaction between ligands and HER2-expressing SKOV-3 cells are presented in Table 1.

The data on the cellular processing and internalization of ^{111}In-DOTA-Cys[2]-ADAPT6 and ^{111}In-DOTA-Cys[59]-ADAPT6 are presented in Figure 2. The rapid binding during the first hour was followed by a slower increase of cell-associated radioactivity. Internalization of the conjugates was relatively slow, below 30% during 24 h for both types of conjugates in both cell lines. Internalization of radioiodinated constructs was not assessed because internalized radioactivity would be severely underestimated in the case of a nonresidualizing label.

In Vivo Studies

The in vivo specificity test demonstrated that tumor accumulation of ^{111}In-DOTA-Cys[59]-ADAPT6 and ^{125}I-HPEM-Cys[59]-ADAPT6 molecules is HER2-mediated (Fig. 3). Presaturation of HER2 in xenografts with trastuzumab decreased the tumor-associated radioactivity significantly ($P < 10^{-5}$).

Data on the biodistribution of ^{111}In-DOTA-Cys2-ADAPT6, ^{111}In-DOTA-Cys[59]-ADAPT6, ^{125}I-HPEM-Cys[2]-ADAPT6, and ^{125}I-HPEM-Cys[59]-ADAPT6 at 1 and 4 h after injection in mice bearing HER2-expressing SKOV-3 xenografts are presented in Tables 2 and 3.

The difference in biodistribution of the radiometal- and the radioiodine-labeled variants was most obvious in the kidneys. In the case of the indium label, the kidney-associated radioactivity was 250%–270% of the injected dose per gram of tissue (%ID/g) at 1 h after injection and did not drop significantly during the following 3 h. In the case of the radioiodine label, at 1 h after injection the renal uptake was still around only 10 %ID/g, and it was further reduced more than 5-fold at 4 h after injection. However, uptake of radioiodine was significantly ($P < 0.05$ in the paired t test) higher in many other organs and tissues. The difference was more pronounced in the case of the C-terminal label.

There was a noticeable difference in biodistribution between ^{111}In-Cys[2]-ADAPT6 and ^{111}In-Cys[59]-ADAPT6 and between ^{125}I-HPEM-Cys[2]-ADAPT6 and ^{125}I-HPEM-Cys[59]-ADAPT6. For example, compared with ^{111}In DOTA-Cys[2]-ADAPT6, ^{111}In-Cys[59]-ADAPT6 showed, at 4 h after injection, significantly lower uptake in the lung and liver and significantly higher uptake in tumor.

TABLE 1
K_D for Interaction of Radiolabeled ADAPT6 Variants with HER2-Expressing SKOV-3 Cells, Determined Using LigandTracer

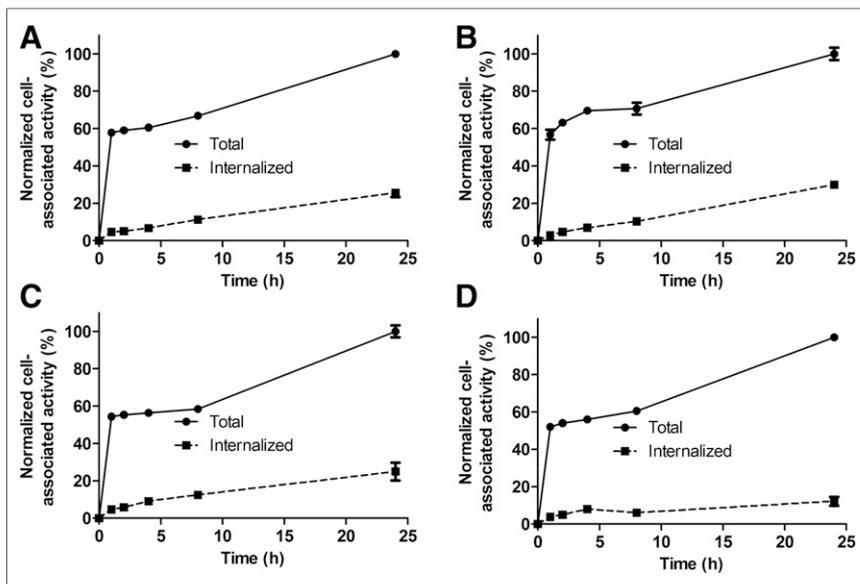| Variant	N terminus		C terminus	
	K_{D1} (pM)	K_{D2} (nM)	K_{D1} (pM)	K_{D2} (nM)
[111]In	212 ± 90	3.6 ± 1.1	188 ± 32	6.6 ± 0.3
[125]I	127 ± 28	11 ± 4	101 ± 12	5.4 ± 2.7

FIGURE 2. Cellular processing of ^{111}In-DOTA-Cys[2]-ADAPT6 (A and B) and ^{111}In-DOTA-Cys[59]-ADAPT6 (C and D) after binding to HER2-expressing SKOV-3 (A and C) and BT474 (B and D) cells. Data are presented as mean with SD from 3 cell dishes.

Tumor uptake was significantly ($P < 0.05$ in the paired t test) higher for the radioiodine-labeled variants at all time points. This difference was more pronounced when the label was at the C terminus. There was no difference in tumor uptake between 1 and 4 h after injection for either ^{111}In or ^{125}I labels when placed at the C terminus. Positioned at the N terminus, both ^{111}In and ^{125}I labels showed a significant reduction in tumor uptake at later time points.

The influence of the nature of the label on tumor-to-organ ratios was also dependent on the label's position. In the case of C-terminal placement, the radiometal label provided significantly increased tumor-to-organ ratios (except for the kidneys) at both time points compared with the radiohalogen label. In the case of N-terminal placement, the use of ^{111}In provided higher ratios than the use of ^{125}I for tumor-to-liver, tumor-to-stomach, and tumor-to-blood (only at 4 h after injection) ratios. ^{111}In-DOTA-Cys[59]-ADAPT6 had significantly ($P < 0.05$) increased tumor-to-lung, tumor-to-liver, tumor-to-spleen, and tumor-to-muscle ratios compared with ^{111}In-DOTA-Cys[2]-ADAPT6. In the case of the radioiodine label,

N-terminal positioning provided significantly ($P < 0.05$) higher tumor-to-blood, tumor-to-lung, and tumor-to-bone ratios at 1 h after injection. There were no significant differences between most tumor-to-organ ratios for radioiodinated variants at 4 h after injection. ^{125}I-HPEM-Cys[59]-ADAPT6 had approximately twice the tumor-to-kidney ratio of ^{125}I-HPEM-Cys[2]-ADAPT6.

The results of the assessment of blood-borne radioactivity in the high-molecular-weight fraction are presented in Supplemental Table 1. For radiometal labeling, components with a molecular weight of over 5 kDa constituted more than 90% of the total radioactivity. For radioiodine labeling, the average radioactivity in the high-molecular-weight fraction was 55%–60%.

Small-animal SPECT/CT imaging of HER2-expressing xenografts in mice using radiolabeled ADAPT6 variants is presented in Figure 4. Renal uptake of ^{111}In-labeled ADAPT6 was much higher than uptake of the ^{125}I-labeled counterparts in SKOV-3 xenografts (Figs. 4A–4D). Figures 4B and 4D show that ^{125}I-HPEM-Cys[2]-ADAPT6 and ^{125}I-HPEM-Cys[59]-ADAPT6 can provide a higher accumulation in HER2-expressing ovarian cancer tumors than in the kidneys. Accumulation of ^{125}I activity in the gastrointestinal tract was visible for both N- and C-terminal placement of ^{125}I-HPEM but was appreciably lower than accumulation in tumors. In addition, there was some accumulation of ^{125}I in the neck region in the case of ^{125}I-HPEM-Cys[59]-ADAPT6.

DISCUSSION

One goal of this study was to test the hypothesis that use of a nonresidualizing label for ADAPT6 would minimize kidney-associated radioactivity without substantially decreasing tumor uptake. Earlier, we demonstrated that use of nonresidualizing radioiodine labels appreciably reduces the renal retention of Affibody molecules (24), and the use of site-specific labeling by HPEM resulted in more efficient clearance of radioactivity from the kidneys than did labeling by conjugation of iodobenzoate (21). In this study, use of the ^{125}I-HPEM label also resulted in a rapid reduction in renal radioactivity (Table 2). Use of HPEM was even more favorable for ADAPT than for Affibody molecules. For Affibody molecules, renal uptake in BALB/C *nu/nu* mice was 16.8 ± 2.3 and 4.5 ± 0.4 %ID/g at 1 and 4 h, respectively (21). For ADAPT6, renal uptake at these time points was 10 ± 2 and 1.7 ± 0.3 %ID/g, respectively, independent of label position. Tumor uptake was not decreased by the use of a nonresidualizing label, as might be expected for a slowly internalized probe. Surprisingly, a paired t test demonstrated significantly higher tumor uptake of ^{125}I than of [111]In (Table 2).
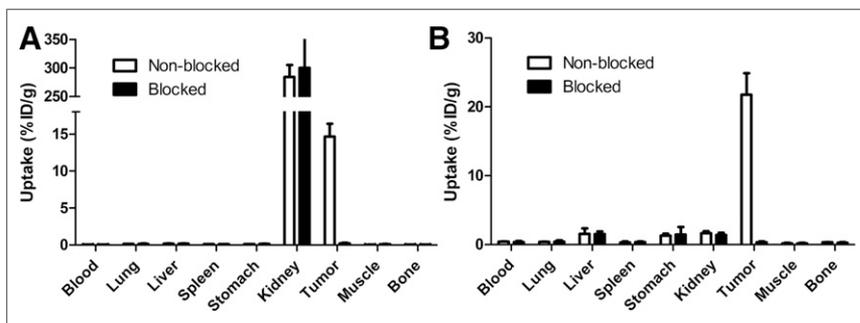

FIGURE 3. In vivo tumor uptake specificity of ^{111}In-DOTA-Cys[59]-ADAPT6 (A) and ^{125}I-HPEM-Cys[59]-ADAPT6 (B) in SKOV-3 xenografts. To saturate HER2 receptors in tumors, one group of animals was preinjected with 15 mg of trastuzumab 24 h before injection of radiolabeled conjugate (designated as blocking). Data are expressed as %ID/g and are averages from 4 animals ± SD.

TABLE 2
Biodistribution of Radiolabeled ADAPT6 in BALB/C *nu/nu* Mice Bearing SKOV-3 Xenografts

Site	^{111}In-DOTA-Cys^{59}-ADAPT6	^{125}I-HPEM-Cys^{59}-ADAPT6	^{111}In-DOTA-Cys^{2}-ADAPT6	^{125}I-HPEM-Cys^{2}-ADAPT6
1 h				
Blood	0.35 ± 0.06*,†	1.0 ± 0.1*,§	0.48 ± 0.10‡,¶	0.54 ± 0.14‡,§
Lung	0.46 ± 0.06*,†	1.4 ± 0.2*,§	0.5 ± 0.1‡,¶	0.6 ± 0.1‡,§
Liver	0.21 ± 0.03†	2.7 ± 0.8	0.26 ± 0.05¶	2.4 ± 0.7‡
Spleen	0.14 ± 0.02*,†,§	0.7 ± 0.2*,§	0.23 ± 0.06‡,¶	0.45 ± 0.04‡,§
Stomach	0.23 ± 0.03*,†	1.6 ± 0.3	0.25 ± 0.07‡,¶	1.2 ± 0.3‡
Kidney	272 ± 21†	10 ± 2*	258 ± 27¶	10 ± 3
Tumor	13 ± 2†	19 ± 3	14 ± 3¶	16 ± 3
Muscle	0.10 ± 0.02*,†	0.34 ± 0.03*,§	0.10 ± 0.05‡,¶	0.2 ± 0.1‡,§
Bone	0.21 ± 0.05*,†	0.9 ± 0.2*,§	0.22 ± 0.04‡	0.31 ± 0.08‡,§
4 h				
Blood	0.053 ± 0.004†	0.41 ± 0.06§	0.04 ± 0.01¶	0.20 ± 0.05§
Lung	0.13 ± 0.03†,§	0.39 ± 0.05§	0.19 ± 0.02¶	0.17 ± 0.04§
Liver	0.17 ± 0.02§	1.6 ± 0.8	0.22 ± 0.01	0.6 ± 0.3
Spleen	0.10 ± 0.00	0.3 ± 0.2	0.12 ± 0.01	0.15 ± 0.03
Stomach	0.10 ± 0.01†	1.3 ± 0.3	0.09 ± 0.02¶	0.8 ± 0.4¶
Kidney	284 ± 21†	1.7 ± 0.3	241 ± 32¶	1.7 ± 0.3
Tumor	15 ± 2†,§	22 ± 3§	10.6 ± 0.5¶	11.8 ± 0.5§
Muscle	0.04 ± 0.01†	0.18 ± 0.08	0.046 ± 0.005	0.09 ± 0.04
Bone	0.07 ± 0.02†	0.31 ± 0.06*,§	0.07 ± 0.02	0.12 ± 0.06§

*Significant difference between uptake of Cys^{59}-ADAPT6 at 1 and 4 h after injection.
†Significant difference between uptake of Cys^{59}-ADAPT6 labeled with ^{111}In and ^{125}I at same time point.
‡Significant difference between uptake of Cys^{2}-ADAPT6 at 1 and 4 h after injection.
¶Significant difference between uptake of Cys^{2}-ADAPT6 labeled with ^{111}In and ^{125}I at same time point.
§Significant difference between uptake of Cys^{59}-ADAPT6 and Cys^{2}-ADAPT6 at same time point.
Data are average %ID/g with SD for 4 animals.

However, use of the ^{125}I-HPEM label was not the only advantage. Radioactivity uptake in most tissues was significantly higher for radioiodine (Table 2), resulting in significantly lower tumor-to-organ ratios (Table 3). Analysis of blood (Supplemental Table 1) suggests that the much higher fraction of radioactivity in blood was associated with a low-molecular-weight fraction (<5 kDa) in the case of the ^{125}I-HPEM labeling. It is likely that this fraction represents renal radiometabolites, which are redistributed through blood into other tissues. Still, the tumor-to-organ ratios at 4 h after injection (Table 3) were appreciably higher than values that ever could be obtained using radiolabeled monoclonal antibodies (*25*). High uptake and good retention of ^{125}I-HPEM-Cys^{59}-ADAPT6 in tumors and its rapid clearance from the kidneys suggest that its ^{131}I-labeled analog might be considered for radionuclide therapy. Of course, an extended study is required to assess absorbed doses in tumors and in normal tissues. The use of a GGGC peptide–based chelator for labeling of Affibody molecules with a β-emitting radionuclide, ^{188}Re (half-life, 17.0 h), provided a nonresidualizing radiometal label with good retention in tumors and low retention in the kidneys (*26*). It would be interesting to evaluate such labeling chemistry for ADAPT as well.

The position of the label influenced the biodistribution of both ^{111}In- and ^{125}I-labeled variants (Table 2). For the ^{111}In-DOTA labels, the influence was limited to significantly reduced uptake in the lung and liver at 4 h after injection. Elevated uptake in these organs is often associated with lipophilicity of the targeting peptides. The (HE)$_3$DANS sequence provides hydrophilicity to the N terminus, and it is possible that conjugation of a hydrophilic chelate at the C terminus increased the overall hydrophilicity of the construct, affecting hepatic and pulmonary uptake. Interestingly, better retention of radioactivity in tumors could be detected for ^{111}In-DOTA-Cys^{59}-ADAPT6 than for ^{111}In-DOTA-Cys^{2}-ADAPT6. The nature of this phenomenon is not clear, as the affinities of both variants are similar (Table 1). However, it has been shown that the relative abundance of high- and low-affinity binding sites for HER receptors is affected by homo- and heterodimerization, which in turn depend on the culturing conditions (*27*). It is possible that the in vivo conditions result in different dimerization patterns, triggering a shift to low-affinity binding sites for conjugates bearing the label at the N terminus. Overall, placement of the ^{111}In-DOTA label at the C terminus provided appreciably higher tumor-to-lung, tumor-to-liver, tumor-to-spleen, and tumor-to-muscle ratios, indicating that this position is better for labeling. Supplemental Table 2 compares the literature data on targeting of SKOV-3 xenografts in immunodeficient mice using several radiometal-labeled HER2-specific probes. The current data suggest that ^{111}In-DOTA-Cys^{59}-ADAPT6 provides the best tumor-to-blood and tumor-to-liver ratios, as well as very good tumor uptake.

TABLE 3
Tumor-to-Organ Ratios of Radiolabeled ADAPT6 in BALB/C *nu/nu* Mice Bearing SKOV-3 Xenografts

Site	^{111}In-DOTA-Cys^{59}-ADAPT6	^{125}I-HPEM-Cys^{59}-ADAPT6	^{111}In-DOTA-Cys^2-ADAPT6	^{125}I-HPEM-Cys^2-ADAPT6
1 h				
Blood	38 ± 3*,†,§	18.8 ± 0.8*,§	28 ± 2‡,¶	31 ± 3‡
Lung	29.4 ± 4.0*,†	13.1 ± 0.7*,§	26 ± 4‡,¶	28 ± 2‡
Liver	64 ± 10†	7 ± 1	53 ± 5¶	7 ± 2‡
Spleen	94 ± 12*,†,§	27 ± 4*	59 ± 11‡,¶	37 ± 9‡
Stomach	59 ± 6*,†	12 ± 1*	56 ± 9‡,¶	14 ± 2
Kidney	0.049 ± 0.003†	1.9 ± 0.2*	0.05 ± 0.01¶	1.6 ± 0.2‡
Muscle	144 ± 37*,†	54 ± 7*	111 ± 9‡,¶	79 ± 29
Bone	66 ± 11†	22 ± 5*,§	62 ± 4‡,¶	54 ± 4‡
4 h				
Blood	277 ± 35†	53 ± 10*	254 ± 37¶	61 ± 14‡
Lung	119 ± 35*,†,§	56 ± 3	55 ± 6‡,¶	73 ± 14‡
Liver	85 ± 17†,§	17 ± 9	48 ± 3¶	24 ± 12‡
Spleen	132 ± 4*,†,§	59 ± 12*	93 ± 7‡,¶	82 ± 15‡
Stomach	147 ± 24*,†	17 ± 2*	116 ± 19‡,¶	17 ± 8
Kidney	0.05 ± 0.01†	13 ± 3*,§	0.04 ± 0.01¶	7 ± 1‡
Muscle	343 ± 85†,§	134 ± 43*	231 ± 18‡,¶	158 ± 63
Bone	246 ± 163	72 ± 21*	152 ± 42‡,¶	119 ± 45‡

*Significant difference between values for Cys^{59}-ADAPT6 at 1 and 4 h after injection.

†Significant difference (paired *t* test) between values for Cys^{59}-ADAPT6 labeled with ^{111}In and ^{125}I at same time point.

‡Significant difference between values for Cys^2-ADAPT6 at 1 and 4 h after injection.

¶Significant difference (paired *t* test) between values for Cys2-ADAPT6 labeled with ^{111}In and ^{125}I at same time point.

§Significant difference between values for Cys^{59}-ADAPT6 and Cys^2-ADAPT6 at same time point.

Data are average %ID/g with SD for 4 animals.

The influence of the label position was also pronounced for ^{125}I-HPEM. With C-terminal placement, there was slower clearance from blood, lung, and bone but also significantly higher tumor uptake at 4 h after injection. This difference cannot be explained by different rates for the appearance of renal radiometabolites in the blood, as the decrease in kidney-associated activity has the same rate for both ^{125}I-HPEM-Cys^2-ADAPT6 and ^{125}I-HPEM-Cys^{59}-ADAPT6. The iodo-HPEM is rather hydrophobic (theoretic log, 2.46), and its conjugation increases the local hydrophobicity of the protein. In the case of N-terminal placement, the hydrophilic (HE)$_3$DANS sequence might be able to compensate for this hydrophobicity. When the label is positioned in the C terminus (next to the sequence ILHALP), the additional hydrophobicity is not compensated for and might increase transient binding to blood proteins. This effect would slow the clearance somewhat and increase the bioavailability of ^{125}I-HPEM-Cys^{59}-ADAPT6, facilitating its higher tumor uptake. Overall, the tumor-to-organ ratios are quite similar for ^{125}I-HPEM-Cys^2-ADAPT6 and ^{125}I-HPEM-Cys^{59}-ADAPT6, but ^{125}I-HPEM-Cys^{59}-ADAPT6 has an advantage of higher tumor uptake and a higher tumor-to-kidney ratio.

FIGURE 4. Small-animal SPECT/CT imaging of HER2-expressing xenografts using ADAPT6 molecules at 4 h after injection (maximum-intensity projections). (A and C) Imaging using ^{111}In-DOTA-Cys^2-ADAPT6 and ^{111}In-DOTA-Cys^{59}-ADAPT6. Linear color scale was adjusted to provide clear visualization of tumors. (B and D) Imaging using ^{125}I-HPEM-Cys^2-ADAPT6 and ^{125}I-HPEM-Cys^{59}-ADAPT6. Full linear color scale was applied.

CONCLUSION

The residualizing properties of the label strongly influence the targeting properties of ADAPT6 and, very likely, other engineered scaffold proteins. The position of the radiolabel influences targeting as well,
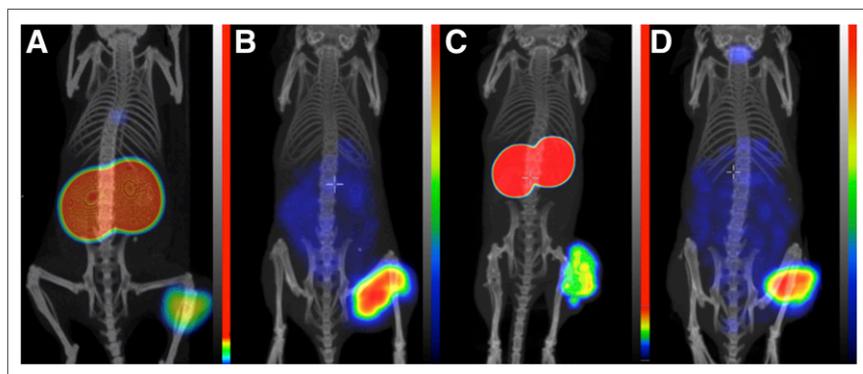
although to a lesser extent. Placement of the label at the C terminus of ADAPT proteins yields the best biodistribution features for both radiometal and radiohalogen labels.

DISCLOSURE

REFERENCES

1. Scott AM, Wolchok JD, Old LJ. Antibody therapy of cancer. *Nat Rev Cancer.* 2012;12:278–287.
2. Mankoff DA. Molecular imaging to select cancer therapy and evaluate treatment response. *Q J Nucl Med Mol Imaging.* 2009;53:181–192.
3. Tolmachev V, Stone-Elander S, Orlova A. Radiolabelled receptor-tyrosine-kinase targeting drugs for patient stratification and monitoring of therapy response: prospects and pitfalls. *Lancet Oncol.* 2010;11:992–1000.
4. Jauw YW, Menke-van der Houven van Oordt CW, Hoekstra OS, et al. Immuno-positron emission tomography with zirconium-89-labeled monoclonal antibodies in oncology: what can we learn from initial clinical trials? *Front Pharmacol.* 2016;7:131.
5. Wester H-J, Kessler H. Molecular targeting with peptides or peptide-polymer conjugates: just a question of size? *J Nucl Med.* 2005;46:1940–1945.
6. Sörensen J, Sandberg D, Sandström M, et al. First-in-human molecular imaging of HER2 expression in breast cancer metastases using the ^{111}In-ABY-025 affibody molecule. *J Nucl Med.* 2014;55:730–735.
7. Sörensen J, Velikyan I, Sandberg D, et al. Measuring HER2-receptor expression in metastatic breast cancer using [68Ga] ABY-025 Affibody PET/CT. *Theranostics.* 2016;6:262–271.
8. Goldstein R, Sosabowski J, Livanos M, et al. Development of the designed ankyrin repeat protein (DARPin) G3 for HER2 molecular imaging. *Eur J Nucl Med Mol Imaging.* 2015;42:288–301.
9. Ackerman SE, Currier NV, Bergen JM, Cochran JR. Cystine-knot peptides: emerging tools for cancer imaging and therapy. *Expert Rev Proteomics.* 2014; 11:561–572.
10. Garousi J, Lindbo S, Nilvebrant J, et al. ADAPT, a novel scaffold protein-based probe for radionuclide imaging of molecular targets that are expressed in disseminated cancers. *Cancer Res.* 2015;75:4364–4371.
11. Nilvebrant J, Hober S. The albumin-binding domain as a scaffold for protein engineering. *Comput Struct Biotechnol J.* 2013;6:e201303009.
12. Wolff AC, Hammond MEH, Hicks DG, et al. Recommendations for human epidermal growth factor receptor 2 testing in breast cancer: American Society

of Clinical Oncology/College of American Pathologists clinical practice guideline update. *J Clin Oncol.* 2013;31:3997–4013.
13. Garousi J, Lindbo S, Honarvar H, et al. Influence of the N-terminal composition on targeting properties of radiometal-labeled anti-HER2 scaffold protein ADAPT6. *Bioconjug Chem.* 2016;27:2678–2688.
14. Lindbo S, Garousi J, Åstrand M, et al. Influence of histidine-containing tags on the biodistribution of ADAPT scaffold proteins. *Bioconjug Chem.* 2016;27:716–726.
15. Froidevaux S, Calame-Christe M, Schuhmacher J, et al. A gallium-labeled DOTA-α-melanocyte-stimulating hormone analog for PET imaging of melanoma metastases. *J Nucl Med.* 2004;45:116–123.
16. Tolmachev V, Hofström C, Malmberg J, et al. HEHEHE-tagged affibody molecule may be purified by IMAC, is conveniently labeled with [99(m)Tc(CO)$_3$]+, and shows improved biodistribution with reduced hepatic radioactivity accumulation. *Bioconjug Chem.* 2010;21:2013–2022.
17. Perols A, Honarvar H, Strand J, et al. Influence of DOTA chelator position on biodistribution and targeting properties of ^{111}In-labeled synthetic anti-HER2 affibody molecules. *Bioconjug Chem.* 2012;23:1661–1670.
18. Honarvar H, Strand J, Perols A, et al. Position for site-specific attachment of a DOTA chelator to synthetic Affibody molecules has a different influence on the targeting properties of ^{68}Ga-compared to ^{111}In-labeled conjugates. *Mol Imaging.* 2014;13:7290201400034.
19. Tolmachev V, Orlova A, Lundqvist H. Approaches to improve cellular retention of radiohalogen labels delivered by internalising tumour-targeting proteins and peptides. *Curr Med Chem.* 2003;10:2447–2460.
20. Mume E, Orlova A, Larsson B, et al. Evaluation of ((4-hydroxyphenyl) ethyl) maleimide for site-specific radiobromination of anti-HER2 affibody. *Bioconjug Chem.* 2005;16:1547–1555.
21. Tolmachev V, Mume E, Sjöberg S, Frejd FY, Orlova A. Influence of valency and labelling chemistry on in vivo targeting using radioiodinated HER2-binding Affibody molecules. *Eur J Nucl Med Mol Imaging.* 2009;36:692–701.
22. Wållberg H, Orlova A. Slow internalization of anti-HER2 synthetic affibody monomer ^{111}In-DOTA-ZHER2: 342-pep2: implications for development of labeled tracers. *Cancer Biother Radiopharm.* 2008;23:435–442.
23. Björkelund H, Gedda L, Barta P, Malmqvist M, Andersson K. Gefitinib induces epidermal growth factor receptor dimers which alters the interaction characteristics with ^{125}I-EGF. *PLoS One.* 2011;6:e24739.
24. Feldwisch J, Tolmachev V. Engineering of affibody molecules for therapy and diagnostics. *Methods Mol Biol.* 2012;899:103–126.
25. Tolmachev V. Imaging of HER-2 overexpression in tumors for guiding therapy. *Curr Pharm Des.* 2008;14:2999–3019.
26. Altai M, Wållberg H, Honarvar H, et al. [188]Re-ZHER2:V2, a promising Affibody-based targeting agent against HER2-expressing tumors: preclinical assessment. *J Nucl Med.* 2014;55:1842–1848.
27. Björkelund H, Gedda L, Malmqvist M, Andersson K. Resolving the EGF-EGFR interaction characteristics through a multiple-temperature, multiple-inhibitor, real-time interaction analysis approach. *Mol Clin Oncol.* 2013;1:343–352.